REPORT DOCUMENTATION PAGE

Form Approved
OMB No. 0704-0188

1. REPORT DATE *(DD-MM-YYYY)*	2. REPORT TYPE	3. DATES COVERED *(From - To)*
31-03-2016	Final Report	From 1 May 2011 to 31 Dec 2015

4. TITLE AND SUBTITLE
COMPONENTS, ASSEMBLY AND ELECTROCHEMICAL PROPERTIES OF THREE-DIMENSIONAL BATTERY ARCHITECTURES

5a. CONTRACT NUMBER

5b. GRANT NUMBER
N00014-11-1-0673

5c. PROGRAM ELEMENT NUMBER

6. AUTHOR(S)
Dunn, Bruce, S (Professor)

5d. PROJECT NUMBER

5e. TASK NUMBER

5f. WORK UNIT NUMBER

7. PERFORMING ORGANIZATION NAME(S) AND ADDRESS(ES)
University of California at Los Angeles (UCLA)
Department of Materials Science and Engineering
420 Westwood Plaza
Los Angeles, CA 90095-1595

8. PERFORMING ORGANIZATION REPORT NUMBER

9. SPONSORING/MONITORING AGENCY NAME(S) AND ADDRESS(ES)
Office of Naval Research
140 Sylvester Road
Bldg. 140, Room 218
San Diego, CA 92106-3521

10. SPONSOR/MONITOR'S ACRONYM(S)
ONR

11. SPONSOR/MONITOR'S REPORT NUMBER(S)

12. DISTRIBUTION/AVAILABILITY STATEMENT
Approved for public release; distribution is unlimited.

13. SUPPLEMENTARY NOTES
None

14. ABSTRACT
In this research program, we advanced 3-D battery technology through a combination of battery design, component development, and improved understanding of electrochemical properties. Our research on liquid polysulfide catholytes emphasized high concentration systems and wider operating potential regimes in order to increase energy density. We also prepared inorganic gels consisting of nanoscale silica networks that have lithium polysulfide catholyte filling the pores. Another key result was the fabrication of a cathode into a 3-D structure which is compatible with the silicon/SU-8 fabrication process. Finally, we assembled a full 3-D battery device and demonstrated charge and discharge cycling in the prototype.

15. SUBJECT TERMS
Three-dimensional battery (3-D battery), 3-D electrode arrays, silicon arrays, photopatternable materials, lithium cycling, polysulfide catholyte, SU-8 electrolyte

16. SECURITY CLASSIFICATION OF:			17. LIMITATION OF ABSTRACT	18. NUMBER OF PAGES	19a. NAME OF RESPONSIBLE PERSON
a. REPORT	b. ABSTRACT	c. THIS PAGE			Bruce Dunn
					19b. TELEPHONE NUMBER *(Include area code)*
U	U	U	UU	11	310-825-1519

OFFICE OF NAVAL RESEARCH

FINAL REPORT

For

Grant Award: N00014-11-1-0673

COMPONENTS, ASSEMBLY AND ELECTROCHEMICAL PROPERTIES OF THREE-DIMENSIONAL BATTERY ARCHITECTURES

Principal Investigator: Bruce Dunn

Department of Materials Science and Engineering
University of California, Los Angeles
Los Angeles, CA 90095-1595

March, 2016

COMPONENTS, ASSEMBLY AND ELECTROCHEMICAL PROPERTIES OF THREE-DIMENSIONAL BATTERY ARCHITECTURES

Award Number: N00014-11-1-0673

1. *Research Objectives*

The overarching theme for the proposed research is to advance 3-D battery technology through a combination of battery design, component development and improved understanding of electrochemical properties. One key aspect for the proposed research is the recognition that liquid components, whether as an electrolyte or catholyte, are advantageous for 3-D batteries. The liquid establishes excellent electrical contact along the length of the rods which comprise the electrode array structure which serve as the central design feature for most 3-D battery architectures. The principal research objectives for this program are directed at improving 3-D battery technology for both primary and secondary systems. Our research related to the Zn-air battery addresses the question of whether the electrochemistry of zinc is affected by high aspect ratio electrodes. In this work we investigated whether the fundamental properties of overpotential, corrosion and other electrochemical properties are influenced by the architecture. The research on secondary batteries is directed at our project on 3-D lithium-ion batteries where improvements in materials and fabrication methods are expected to facilitate battery assembly processes as well as lead to enhanced energy storage properties and further advance the technology. Our work on liquid systems for secondary batteries is pursuing improvements in energy density without compromising reversibility. A key research objective is to synthesize the polysulfide catholyte as a gel, which will move us toward solid-state systems which offer improved safety.

During the research program, we recognized that a polymer photoresist capable of supporting Li^+ transport could be a key feature in secondary 3-D battery technology because it could address two important issues: the fabrication of a conformal electrolyte directly on the electrode structure and the ability to use lithographic tools in battery assembly and alignment. As our work on the photo-patternable electrolyte progressed, it became apparent that the carbon-based array electrodes we developed previously were incompatible with the mechanical forces associated with polymer processing and lithographic alignment characteristics. For these reasons, we initiated research on silicon electrode arrays and demonstrated their reversible lithium ion insertion/de-insertion properties. Silicon is completely compatible with the photo-patternable electrolyte and we have successfully deposited this electrolyte onto silicon electrode arrays. Thus, the additional research objectives are described in three integrated areas: (1) Development of a photo-patternable electrolyte; (2) Characterization of silicon electrode arrays and (3) Photo-patterning of a polymer electrolyte on silicon electrode arrays.

2. *Research Highlights*

2.a. *Polysulfide Catholytes and Gels*

During the initial reporting period we made significant progress in several areas. Our research on liquid polysulfide catholytes emphasized high concentration systems (to 1.5 M) and wider operating

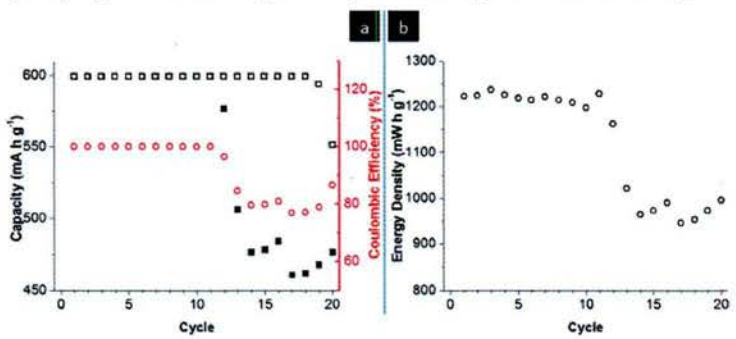

Figure 1: (a) Charge (□) and discharge (■) capacity and coulombic efficiency (○) and (b) energy density (with respect to sulfur mass) of 100mM Li_2S_6 battery with nitrate additive (as 0.4M $LiNO_3$) and 5% MA. Current density: 100 $\mu A \cdot cm^{-2}$. Electrolyte: 0.8M $LiSO_3CF_3$ in TG/DXL (30/70 v/v).

potential regimes in order to increase energy density. Both approaches were successful. Galvanostatic measurements in 2D battery configurations show that 500 mM of polysulfide exhibits high energy density and high Coulombic efficiency. The addition of $LiNO_3$ to the polysulfide suppresses the shuttle mechanism and enables us to extend our system reversibly to $Li_2S_{2.5}$, increasing the energy density further. The use of methylene acetate as a second additive leads to improvements as well. Using both additives, the resulting 2D Li/polysulfide batteries exhibit gravimetric energy densities of 550 to 600 mAh g^{-1} with nearly 100% coulombic efficiency and very good cycling stability. These results are summarized in Figure 1.

Related to this effort is our work on the synthesis of polysulfide gels. Using the sol-gel process, we have now prepared inorganic gels consisting of nanoscale SiO_2 networks that have lithium polysulfide catholyte filling the pores. To our knowledge, this is the first time that catholyte materials have been prepared as a sol-gel material. Despite being a macroscopic solid, from an electrochemical standpoint, the material behaves as a liquid polysulfide. Voltammetric sweeps show stable redox behavior with charge transfer occurring similarly to that of liquid polysulfides, while galvanostatic measurements (Figure 2) indicate typical charge-discharge battery performance when using lithium and molybdenum foils as electrodes.

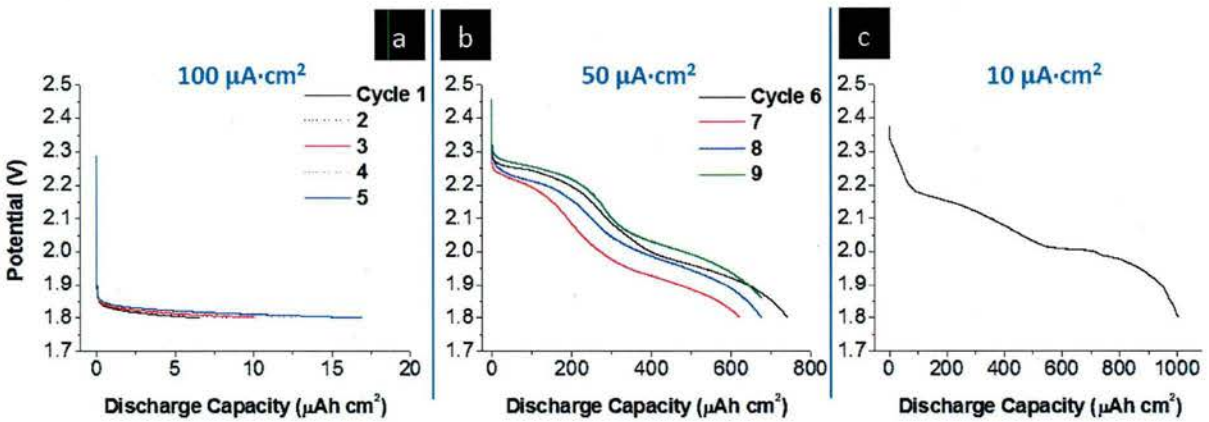

Figure 2: GCPL discharge profiles of 250mM Li_2S_6 sol-gel battery at (a) 100 µA·cm^{-2}, (b) 50 µA·cm^{-2}, and (c) 10 µA·cm^{-2}. Electrodes: molybdenum, working; lithium, counter/reference. Electrolyte: 0.4M $LiSO_3CF_3$.

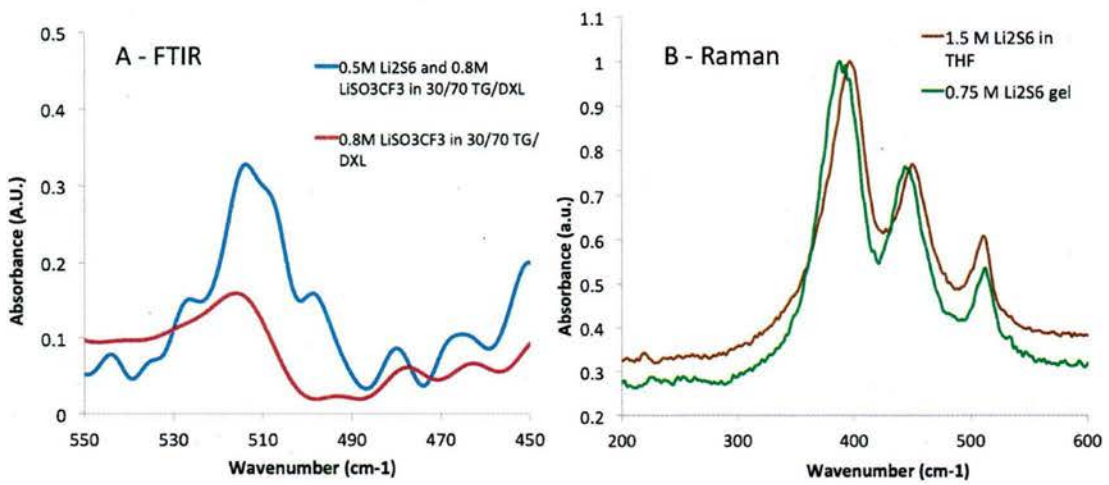

Figure 3 – (a) FTIR spectra of 0.5 M Li_2S_6 catholyte vs. the $LiSO_3CF_3$ supporting electrolyte, both in a 30/70 mixture of tetraglyme and dioxolane. (b) Raman spectra taken from a 1.5 M Li_2S_6 solution in THF and a 0.75 M Li_2S_6 gel.

We also made substantial progress on the synthesis of polysulfide gels where we were able to successfully control the gelation time by varying the polysulfide content. Raman spectroscopy (Figufe 3) studies showed that the sulfur-sulfur bonds in the polysulfide gel were identical to those in the liquid catholyte. This indicates that the encapsulation process does not affect the chemistry of the polysulfide. In addition, we confirmed the ability of this material to undergo reversible charge-discharge reactions and perform as a 'quasi' solid-state battery.

2b. 3D Electrode Arrays

Our research on 3-D electrode arrays emphasized the development of electrode structures for a 3D concentric tube battery that is capable of achieving energy densities on the order of 100 J cm^{-2}. We carried out the fabrication of 3-D array electrodes that effectively meet this design objective; the periodicity of the array architecture enables us to accurately predict mass loading and energy density. Both potentiostatic and galvanostatic cycling experiments showed that the carbon post arrays are capable of reversibly cycling lithium with areal capacities as high as 8 mAh cm^{-2}, consistent with the values calculated by our model. Although the capacity fades with cycling (Figure 4), our areal energy density values are substantially larger than 3-D architectured electrodes found in literature, most of which store much less than 1 mAh cm^{-2} and operate at low current densities. We have identified lithium depletion in the electrolyte to be the principal contributor to capacity fade. Our fabrication process offers the opportunity to tune rod and pitch dimensions, which will enable us to avoid electrolyte depletion and overcome the fading problem.

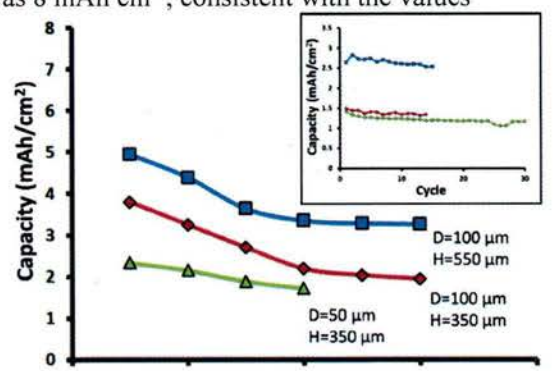

Figure 4: Cycling data of 3D electrodes showing initial capacity fade of electrode 3D-1 (blue), 3D-2 (red) and 3D-3 (green). Inset shows a stable discharge capacity for many cycles after the initial fade.

In our work related to Zn-air primary batteries, we improved our micromachining process to eliminate gas bubbles that form in the narrow and deep holes in the silicon mold. This advance will enable us to improve the quality of the high aspect ratio Zn posts which comprise the Zn electrode arrays. We have also identified a series of polyethylene glycol-based additives that suppress corrosion when Zn is immersed in an alkaline electrolyte. We have further developed the intermittent vacuum degassing method and have begun to establish design rules for extending this technique to a wide variety of patterns.

2.c. Photopatternable Materials and Silicon Arrays

During the second half of the reporting period, we focused on new materials and electrode array fabrication processes for 3-D lithium-ion batteries and made substantial progress. In particular, our research emphasized the development of a new polymer electrolyte that is photo-patternable. Negative photoresist SU-8 3010 was chosen as the new polymer electrolyte because of its wide range of patternable thickness. The use of photo-patterning greatly facilitates the manufacture of microscale electrode arrays which are conformally coated with a polymer electrolyte. Both impedance measurements and galvanostatic cycling experiments have shown that the photo-patterned material is capable of reversibly cycling lithium and serving as an electrolyte in a battery structure (Figure 5). Ionic conductivity values are estimated from impedance measurements were to be ~ 10^{-6} S cm^{-1} for films on the order of 1 µm thick.

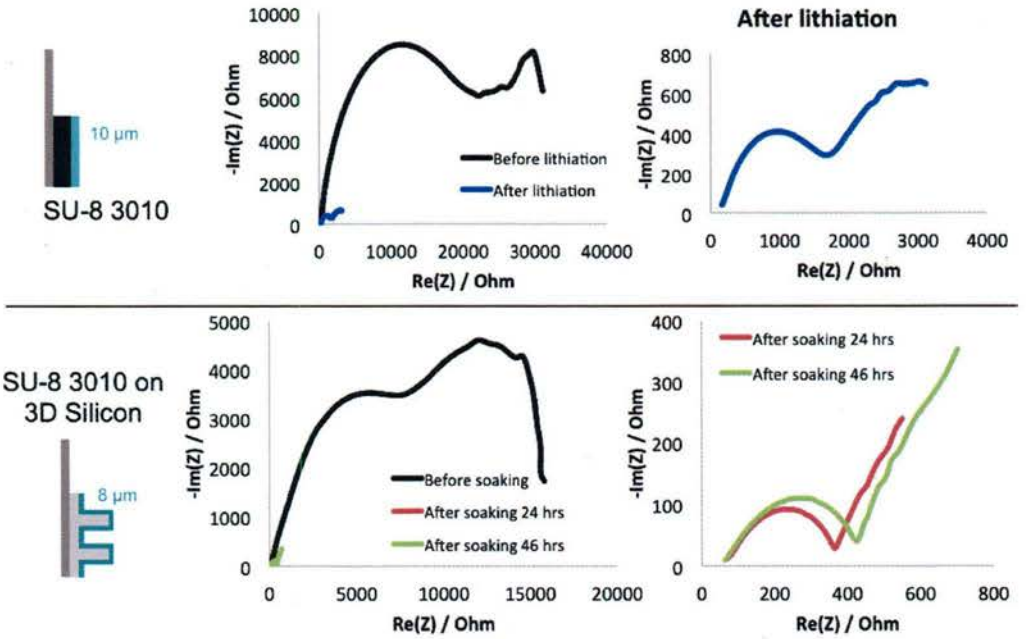

Figure 5 – (Top) drawing of SU-8 3010 on MCMB electrode and EIS data before and after lithiation. (Bottom) EIS data of SU-8 3010 patterned on silicon post array before and after soaking in electrolyte.

In order to successfully pattern the developed electrolyte over the high-aspect-ratio electrode array, a new anode material has been introduced in our 3-D battery project. Although the established carbon post array performs well in liquid electrolytes, it was incompatible with the use of a photo-patternable electrolyte because of light absorption and mechanical integrity. Thus, we began to investigate crystalline silicon post arrays because of their mechanical strength, high energy density, and reflective surface. A silicon post array has been microfabricated and characterized in potentiostatic and galvanostatic experiments (Figure 6).

We have fabricated silicon electrode arrays and carried out lithium cycling experiments. The silicon wafer was patterned and etched to obtain post arrays of 100 µm diameter, 370 µm height, and 75 µm pitch. The silicon posts are connected to each other from a 10-100 µm thick base to form an electrically continuous electrode structure. The array is mounted on stainless steel foil with silver paste for electrical conduction. Half-cell cycling of the mounted silicon array chip in 1M $LiClO_4$ electrolyte with 50:50 EC/DMC confirmed that after 4 cycles of 10% lithiation, the posts are still shiny and in place without any observable damage.

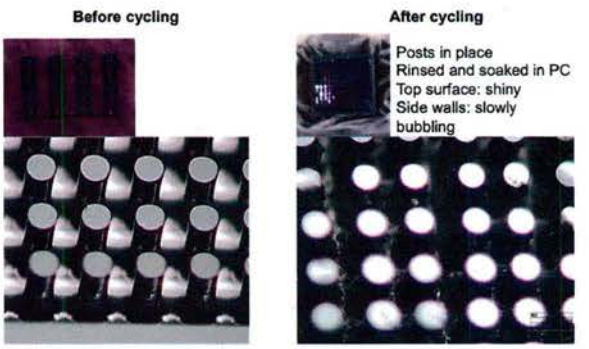

Figure 6 – Optical images of mechanically stable silicon post array before and after galvanostatic cycling to 10% of its theoretical capacity limit.

By limiting the amount of lithiation, it is possible to avoid the well-known degradation problems with silicon and still provide sufficient capacity to meet our 100 J/cm^2 goal. Patterning of this new electrolyte onto the fabricated silicon post array has been successful (Figure 7). The combination of the

silicon array and a photo-patternable electrolyte represents a significant improvement in battery fabrication and is expected to facilitate the assembly of a full 3-D lithium-ion battery system.

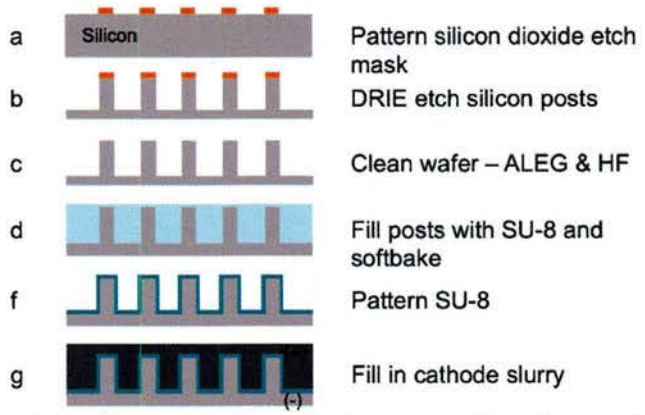

Figure 7 – Process flow of 3-D silicon anode electrode, photopatternable polymer resist, and cathode assembly.

We followed up on our initial results for the photo-patternable polymer (SU-8) with a more in-depth study regarding the effect of cross-linking on ionic conductivity. FTIR was used to characterize the chemical changes arising from UV photo-polymerization of the monomer (Figure 8). The degree of cross-linking had only a short-term effect, possibly because the SU-8 ionic conductivity was dependent upon immersion in electrolyte. Regardless of the amount of cross-linking, conductivity values were in the range of 10^{-7} S cm^{-1}; having such a wide processing window is advantageous for our assembly methods.

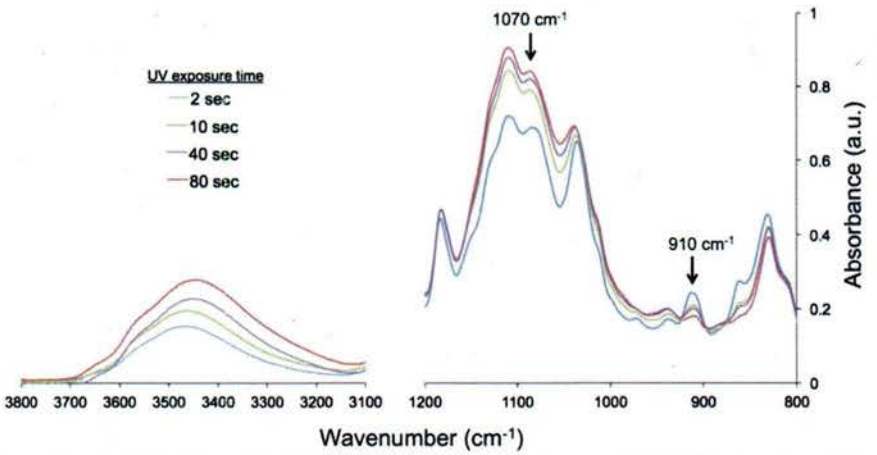

Figure 8 – FTIR curves for SU-8 on NaCl plates exposed to UV for various times.

Another key result was the fabrication of a cathode into a 3-D structure which is compatible with the silicon/SU-8 fabrication process. Using vacuum infiltration, the cathode slurry effectively filled the region between polymer-coated silicon pillars, providing that an appropriate concentration of solid was in the slurry. The cathode material we selected is the well-known lithium nickel cobalt aluminum oxide (NCA) system. The addition of an ion conducting gel to the slurry improved the electrochemical properties and enabled the cathode to exhibit stable cycling at a current density of 0.5 mA cm^{-2}. The capacity achieved in these experiments was ~130 mAh g^{-1}, which is close to 90% of theoretical for NCA (Figure 9).

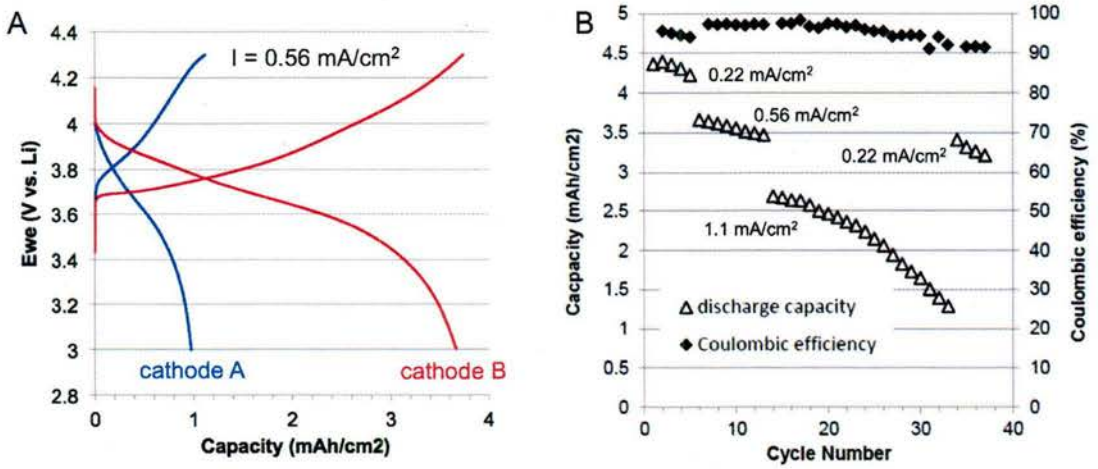

Figure 9 – (a) comparison of first cycle GV performance for Cathode A (no gel electrolyte) and Cathode B (5% LiTFSI:TG:PEO); (b) Capacity and Coulombic efficiency data for extended cycling of Cathode B.

With the successful processing and operation of the 3-D cathode, we now have all the processes in hand to assemble a full 3-D battery. Prior to cathode infiltration, the SU-8 coated silicon array was lithiated in order to condition the silicon and to improve the conductivity of the SU-8. After this step, the cathode slurry was vacuum infiltrated. The initial open circuit voltage of 2.35V is consistent with the expectation of the battery being in its fully discharged state. Unfortunately, this first generation 3-D battery exhibited significant polarization which limited the capacity to ~ 10% of the designed value of 9 mAh cm^{-2}. Nonetheless, the battery operated successfully for several cycles at this lower capacity. In addition to demonstrating battery operation, these initial studies are extremely valuable because they identify the materials, designs and processes requiring improvement.

Fabrication parameters related to the SU-8 coating have been studied extensively during the reporting period. Accordingly, we have established a number of important protocols to ensure reliability (Figure 10). The flatness of the current collector substrate, SU-8 storage, amount of SU-8, soft bake time, UV exposure dose, and development time are critical to obtain uniformly patterned SU-8. We have adopted ITO on glass as the current collector for the negative electrode to ensure the flatness of substrate during UV exposure. The flatness was important due to the very high aspect ratio of SU-8 polymer electrolyte. Since we are patterning 10 μm thick SU-8 over 350 μm tall silicon posts, the aspect ratio is 35:1 and even a slight tilt on the silicon post array can result in there being an unexposed/uncoated area on the post array. The thickness of SU-8 over silicon posts was also important since the patterning is sensitive to the total thickness of SU-8 exposure. After many tests, we have found that 20 hours of soft baking at 100°C dries the SU-8 solvent enough for uniform patterning and SU-8 remains optically clear for UV patterning. The UV exposure dose is 600 mJ/cm^2 for uniform patterning without underexposure or overexposure problems. Exposures less than 560 mJ/cm^2 showed underexposure where SU-8 is not crosslinked at the bottom of the silicon posts and exposures of more than 640 mJ/cm^2 led to overexposure so that SU-8 starts to crosslink at the top surface. By carefully following these key parameters, the lithographically defined electrolyte is uniformly coated over the post array electrode. The thickness we currently use is 10 μm and with further control we expect to achieve 5 μm which will be beneficial because of the lower resistance.

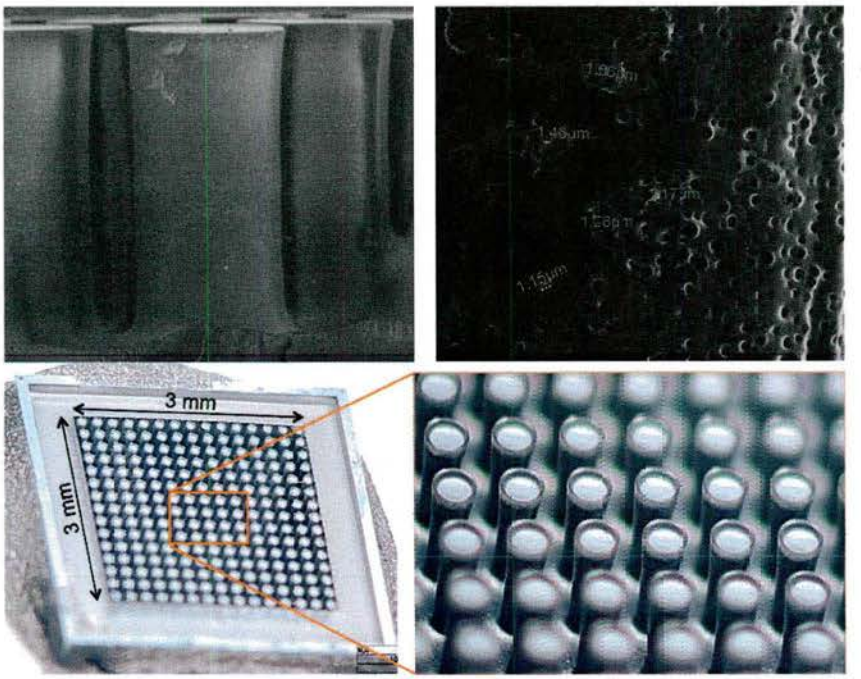

Figure 10 – (Top left) Patterned SU-8 observed under SEM shows uniform coating without bubbles. (Top right) SU-8 surface shows some porosity that is 1 µm. (Bottom left) Whole view of SU-8 patterned silicon array. (Bottom right) SU-8 pattern is well aligned over silicon posts.

We built a simple 2D battery to confirm that the SU-8 electrolyte could function with good electrochemical stability in a full lithium-ion cell. This 2-D battery also provides an indication of what we can expect for the 3-D battery because the materials are the same and the electrolyte thickness is comparable. The cell, shown schematically in Figure 11a, has a high conductivity (0.001 – 0.005 ohm-cm) Si wafer as the anode. The cathode is composed of 75% $LiNi_{0.8}Co_{0.15}Al_{0.05}O_2$ (NCA) with 20% graphite and 5% gel polymer electrolyte (2 : 1 : 1 molar LiTFSI : tetraglyme : polyethylene oxide). 10 µm of SU-8 was coated on the Si wafer, exposed for 40 seconds of UV and soaked for 24 hours before assembling the battery. The total mass of active NCA material is 1 mg over a 0.2 cm^2, corresponding to a capacity of 750 $\mu Ah/cm^2$.

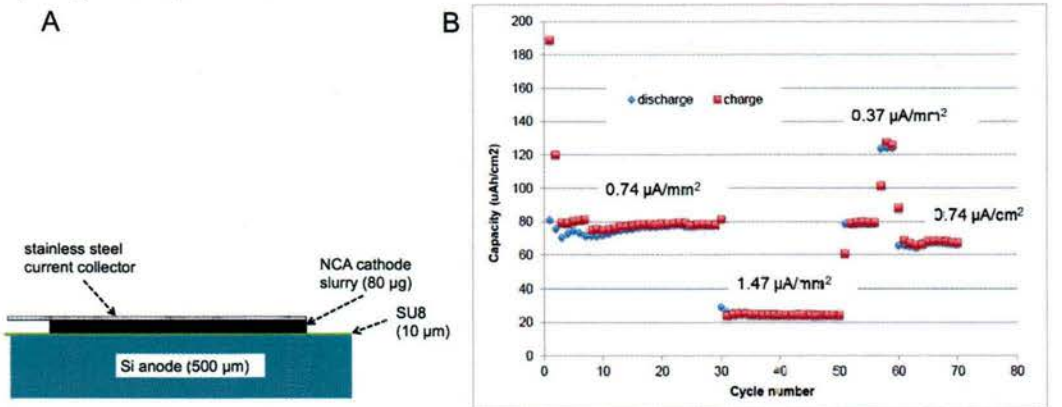

Figure 11 – (a) Schematic of the 2D battery using SU-8 as the electrolyte; (b) capacity data for extended cycling of the 2D battery

The cycling data for the 2D battery is shown in Figure 11b. The capacity is less than the theoretical capacity. However, the coulombic efficiency is very high and there is minimal capacity fade after 70 cycles. The reason that the capacity is below the theoretical value is that the resistance of the cell is simply too high to operate at these currents. At the end of each cycle there is a 5 second pause during which the cell potential relaxes back to its equilibrium potential. The magnitude of the change in voltage during this time is the overpotential. The overpotential increases from about 0.2 V to 0.5 V as the current density increases from 0.37 $\mu A/mm^2$ to 1.47 $\mu A/mm^2$, which corresponds to a cell resistance of about 15 kohms.

After pre-cycling the half-cell, the full 3-D cell was assembled by vacuum infiltrating the cathode slurry. The open circuit potential of the assembled full cell was 2.35 V, which is close to the fully discharged state. Compared to the SU-8 patterned silicon array, the full 3-D cell showed two distinct semi-circles as the ion conductivity through the cathode is probably associated with the increased diameter of the second semi-circle. The calculated total ionic conductivity through the full cell is 3×10^{-7} S/cm.

The 3-D cell was initially operated at a C/20 rate (Figure 12). Thus, 20 hours at 24.5 μA (82.6 $\mu A/cm^2$) was applied to the full cell. Due to the 0.5 V overpotential of the full cell, the voltage limit was shifted 0.4 V more positive during charging and 0.4 more negative during discharging. Moreover, because of irreversible lithiation at high potential, we limited the lithiation time to 5 hours. This corresponds to ~0.8 mAh/cm^2 of discharge from the full 3-D cell, and represents only 10% of the design goal of 9 mAh/cm^2. Nonetheless, as shown in Figure 12, the battery operated for several cycles at this reduced capacity.

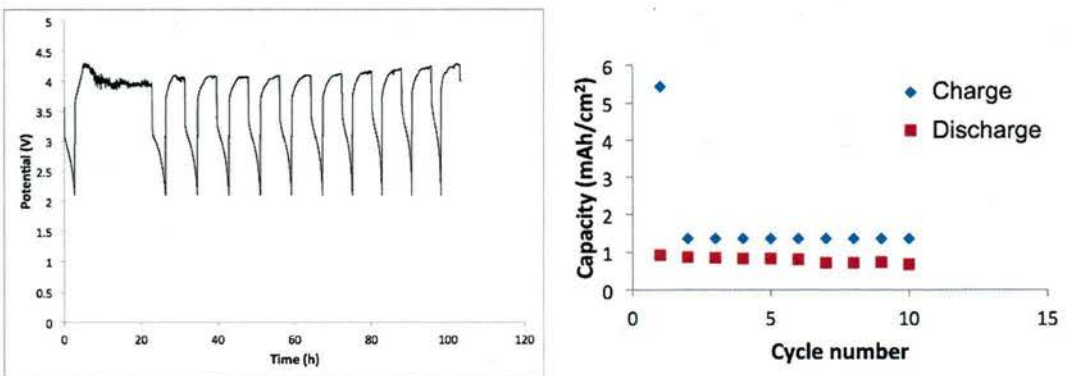

Figure 12 – (Left) Galvanostatic charge and discharge of full cell at C/20 rate. After 5 hours of charging irreversible lithiation occurs and 0.8 mAh/cm^2 discharge capacity was obtained.

The full 3-D cell has been successfully assembled and cycled. It demonstrated the ionic conductivity that is consistent with the impedance study of SU-8. The low energy density of this first device can be improved to reach the target energy density by achieving better cathode filling between the post array and ensuring that the cathode remains ionically conductive throughout charging and discharging. The energy density of the full cell is designed to reach 100 J/cm^2 as shown in Figure 13. Since the silicon post array currently exceeds the target value for areal capacity, the pitch of the silicon array can be increased to accommodate more cathode material for higher energy density. Decreasing the thickness of the SU-8 layer will also be beneficial.

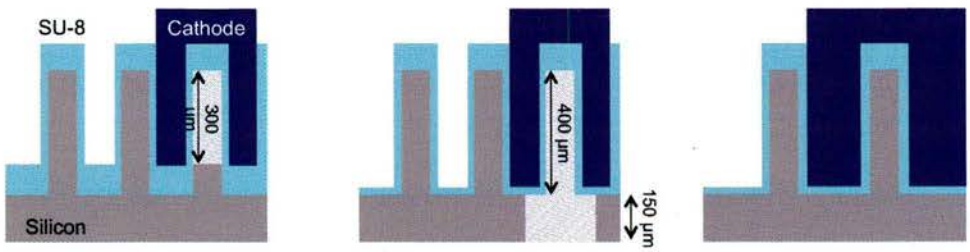

Post diameter	100 µm	Post diameter	100 µm	Post diameter	100 µm
# of posts	17*17	# of posts	17*17	# of posts	15*15
Areal capacity	A: 7.04 mAh/cm² C: 8.07 mAh/cm²	Areal capacity	A: 17.53 mAh/cm² C: 9.71 mAh/cm²	Areal capacity	A: 15.97 mAh/cm² C: 10.42 mAh/cm²
Energy density	5µm: 76 J/cm² 10µm: 76 J/cm²	Energy density	5µm: 105 J/cm² 10µm: 98 J/cm²	Energy density	5µm: 113 J/cm² 10µm: 107 J/cm²

Figure 13 – Energy density calculation of 3-D full cell shows that target energy density can be reached with current design and materials.